PERIODICO di MINERALOGIA
established in 1930

DIPARTIMENTO
DI SCIENZE DELLA TERRA

SAPIENZA
UNIVERSITÀ DI ROMA

An International Journal of
Mineralogy, Crystallography, Geochemistry,
Ore Deposits, Petrology, Volcanology
and applied topics on Environment, Archaeometry and Cultural Heritage

Crystal structure, EMPA and FTIR spectroscopy of green yoderite, $(Mg_{2.02}Al_{5.68}Fe^{3+}_{0.35})_{\Sigma 8.05}(Si_{3.93}P^{5+}_{0.03})_{\Sigma 3.96}O_{18}(OH)_2$, from Mautia Hill, Tanzania

Athos Maria Callegari [1], Massimo Boiocchi [2], Maxwell C. Day [3,*], Frank C. Hawthorne [3]

[1] Department of Earth Sciences and Environment, University of Pavia, via Ferrata 1, I-27100 Pavia, Italy
[2] Centro Grandi Strumenti, University of Pavia, via Bassi 21, I-27100 Pavia, Italy
[3] Department of Geological Sciences, University of Manitoba, Winnipeg, Manitoba R3T 2N2, Canada

ARTICLE INFO

Submitted: September 2021
Accepted: October 2021
Available on line: November 2021

* Corresponding author:
umday23@myumanitoba.ca

Doi: 10.13133/2239-1002/17556

How to cite this article:
Callegari A.M. et al. (2021)
Period. Mineral. 90, 371-381

ABSTRACT

Green yoderite, with the ideal crystal-chemical formula $^{[6]}(MgAl_3)^{[5]}(MgAl)^{[5]}(Al_2)O_2(SiO_4)_4(OH)_2$, from the type locality, Mautia Hill, Tanzania, has been characterized by accurate X-ray diffraction data and crystal-structure refinement at ambient conditions, electron microprobe analysis and FTIR spectroscopy. Yoderite is monoclinic with a=7.9979 (3), b=5.8003 (2), c=7.2299 (2), β=104.7398 (9) Å, V=324.36 (2) Å^3, space group $P2_1/n$ (no. 14), Z=1. Crystal-structure refinement with all non-H atoms refined anisotropically converged to an R_1 value of 2.50% based on all 2089 unique reflections and 94 refined parameters. Chains of edge-sharing A(1)O_5(OH) octahedra extend in the **b** direction and the A(1) site is occupied by 0.75 Al+0.25 Mg. These chains are linked by isolated SiO_4 tetrahedra and by two independent trigonal bipyramids A(2)O_4(OH) and A(3)O_5, where the A(2) site is occupied by 0.50 Al+0.50 Mg and the A(3) site by 0.94 Al+0.06 Fe^{3+}. The hydrogen-bond scheme is established on the basis of the H-atom position observed in the final ΔF map and refined without restraint. Fitting of the FTIR spectrum in the principal (OH)-stretching region shows that $^{A(2)}$Al and $^{A(2)}$Mg are preferentially associated with certain $^{A(1)}$(AlAl), $^{A(1)}$(AlMg) and $^{A(1)}$(MgMg) dimers. Comparison of the band positions, observed intensities and associated local short-range arrangements suggests that the bond valence requirements of such arrangements control the chemical composition of the crystal.

Keywords: green yoderite; Mautia Hill; structure refinement; electron microprobe; FTIR spectroscopy; hydrogen bonds.

INTRODUCTION

Yoderite, ideally $Mg_2Al_6Si_4O_{18}(OH)_2$, was found in a talc-kyanite-quartz 'whiteschist' in the Usagaran Complex, Mautia Hill, Tanzania (McKie, 1959; McKie and Bradshaw, 1966; Mruma and Basu, 1987), where it occurs as both green and purple crystals. This was the only known locality for yoderite until the find by Johnson and Oliver (1998) in whiteschists from the Southern Chewore Hills of Northern Zimbabwe.

Yoderite is a nesosilicate classified in the 52.02 Dana class (Gaines et al., 1997): "insular SiO_4 groups and O, OH, F, and H_2O with cations in [4]- and >[4]-coordination" and is a member of the Al_2SiO_5 andalusite subgroup 52.02.02b. It is structurally related to the nesosilicates kyanite and staurolite as these minerals have crystal structures characterized by alternating layers, one of

which is the Al_2SiO_5 layer in the kyanite structure.

The crystal structure of purple yoderite was solved by Fleet and Megaw (1962) and refined by Higgins et al. (1982) at room temperature before and after heat treatment.

Yoderite has a complex pattern of satellite reflections which are due to structural modulation normal to (010) (McKie, 1959). The superstructure responsible for the satellite reflections was described by Higgins and Ribbe (1977), Ribbe et al. (1981), Lefebvre, (1982) and Higgins et al. (1982) using X-ray diffraction and transmission electron microscopy, and possibly results from long-range order of Mg/Al at the A(1) and A(2) sites and preferential occupancy of the A(3) site by Fe. Heating at 800°C in Ar atmosphere for 15 days, followed by a rapid quench, removed the satellite reflections and resulted in a disordered structure (Higgins et al. 1982). Both purple and green yoderite from the type locality were studied by optical absorption and Mössbauer spectroscopy (Abu-Eid et al., 1978), which established that the two varieties of yoderite have identical Mössbauer spectra, with Fe^{3+}/Fe^{tot}=0.95 and Fe at more than one site. The difference in colour is due to the presence of ~0.08 atoms per formula unit (apfu) of Mn in the purple sample. Yoderite was also examined by Mg *K*-edge XANES as it contains Mg-occupied sites of different coordination number (Li et al., 1999). Furthermore, the stability of yoderite in the MASH system (Schreyer and Seifer, 1969) and as a function of f_{O_2} (Fockenberg and Schreyer, 1991) has been determined.

The available structural parameters of the "ordered" yoderite crystal structure (from an unheated crystal obtained without considering the X-ray satellite reflections) gave an R_1 factor of 6.0% for 1097 relections (Mo$K\alpha$) and the position of the H atom was not established (Higgins et al., 1982). As detailed structural data are required for the FTIR spectroscopic study reported here, we decided to refine the crystal structure of yoderite in more detail at ambient temperature, using green yoderite from the type locality of Mautia Hill. (Figure 1)

EXPERIMENTAL

Chemical data

Preliminary energy-dispersive spectrometry (EDS) was done on a fragment of the same specimen used for the single crystal X-ray diffraction study. A traverse of several points (from core to rim) showed the presence of Si, Al, Mg and minor Fe, Ti, Mn, P as the only elements detected with Z≥8. For EMPA (electron microprobe analysis), samples were mounted in epoxy in an acrylic ring,

Figure 1. Anhedral laths of emerald-green yoderite crystals associated with grey-white aggregates of talc crystals. The sample is stored in the Mineralogical Museum at the University of Pavia under the registration number 8430. Field of view is 0.75 cm.

ground, polished, and carbon coated. EMPA was done with a Cameca SX-100 electron microprobe operated in wavelength-dispersive mode with an accelerating voltage of 15 kV, a beam current of 20 nA and a beam size of 1 μm. The following standards were used for *K*α lines: Mg, forsterite; Al, andalusite; Si, Fe, fayalite; P, apatite; Ti, titanite; Mn, spessartine. Ten analytical points were measured on a fragment of the X-ray crystal and data were corrected using the PAP procedure of Pouchou and Pichoir (1985). The unit formula was calculated on the basis of (O, OH)=20 apfu with (OH)=2 apfu. Compositional data are given in Table 1.

Crystal data and structure-refinement details

Diffraction data were collected from an emerald green, transparent, prismatic single crystal of yoderite, selected for X-ray diffraction analysis based on its optical and diffraction properties, using a Bruker-AXS three-circle diffractometer operating at 50 kV and 30 mA and equipped with the Smart-Apex CCD detector. Data were collected at ambient temperature using graphite-monochromated Mo*K*α radiation with a detector-to-crystal working distance of 50 mm. Details of the data collection and structure refinement are reported in Table 2. Omega-rotation frames were processed by the Saint software (Bruker, 2003) for data reduction, including background, Lorentz and polarization corrections. An empirical absorption correction (SADABS 2016/2, Krause et al., 2015) was applied to the intensity data. Unit-cell parameters were obtained by least-squares refinement from the positions of 6617 reflections with $I > 10\sigma I$ collected in the θ range 2.6-40.0°.

Refinement of the structure was done in space group $P2_1/m$ on F^2 using weighted full-matrix least-squares procedures (SHELXL-2014/7, Sheldrick, 2015), using the atom coordinates and labelling scheme of Higgins et al. (1982). Scattering curves for neutral atoms were taken from the International Tables for X-ray Crystallography, Volume C (Ibers and Hamilton, 1992). Anisotropic-displacement parameters were refined for all non-H atom sites.

As expected, our X-ray diffraction data show a complex pattern of weak and diffuse satellite reflections: simulated X-ray precession maps of the *hk*0 and 0*kl* plane (Figure 2) confirm the features of McKie (1959) that were later emphasized by the electron-diffraction patterns of Higgins et al. (1982). Omitting the superstructure reflections, refinement of the "ordered" structure showed no unusual features and converged to low agreement indexes (Table 2), confirming that the average structure is substantially unaffected by the modulation. In the first steps of the refinement, the A- (Al vs □) (□=vacancy) occupancy was slightly <1 for the A(1) and A(2) sites and >1 for A(3). Mg was assigned to the A(1) and A(2) sites and the s.o.f. (site occupation factors) for these sites were constrained to 0.25Mg+0.75Al at A(1) and 0.50Mg+0.50 Al at A(2), which agrees with our chemical formula (Table 1) and with the refined mean A–O bond distances. Fe was assigned to the A(3) site together with Al and the s.o.f. was freely refined.

The position of the H atom was found in the final difference-Fourier map and was refined without any restraints on atom coordinates and fixing U_{iso} to 1.3 times the value of U_{eq} of the bonded O(8) oxygen atom. The final Δ*F* map was featureless and showed a highest peak and deepest hole of 0.49 *e*/Å^3 and -0.70 *e*/Å^3, respectively. The anisotropic structure refinement converged to final R_1 factors of 2.41% for 1984 reflections with $I/\sigma I \geq 2$ and 2.50% for all 2089 reflections. Atom coordinates, site occupancies and equivalent isotropic-displacement parameters are listed in Table 3, interatomic distances and other selected geometrical and distortion parameters are compiled in Table 4, and anisotropic-displacement parameters are reported in Table 5.

Table 1. Chemical composition (wt%) and unit formula (apfu) for green yoderite.

Oxide	wt (%)	Range		apfu
SiO_2	36.09(33)	35.91-36.38	Si^{4+}	3.93
Al_2O_3	44.17(24)	43.76-44.46	P^{5+}	0.03
MgO	12.45(12)	12.35-12.53	∑T	3.96
Fe_2O_3	4.20(13)	4.10-4.25	Al^{3+}	3.01
P_2O_5	0.28(2)	0.20-0.35	Mg^{2+}	1.01
TiO_2	0.06(4)	0.02-0.11	∑A(1)	4.02
MnO	0.04(4)	0.01-0.05	Al^{3+}	1.01
H_2O*	2.75		Mg^{2+}	1.01
Total	100.04		∑A(2)	2.02
			Al^{3+}	1.66
			Fe^{3+}	0.35
			∑A(3)	2.01

H_2O* was calculated assuming ^{O8}(OH)=2.0 apfu.

Infrared spectroscopy

A single crystal for FTIR (Fourier-transform infrared) analysis was selected based on clarity and uniform extinction under cross-polarized light and then double polished to a thickness of ~45 microns and mounted (unoriented) on a diamond plate. An FTIR spectrum was

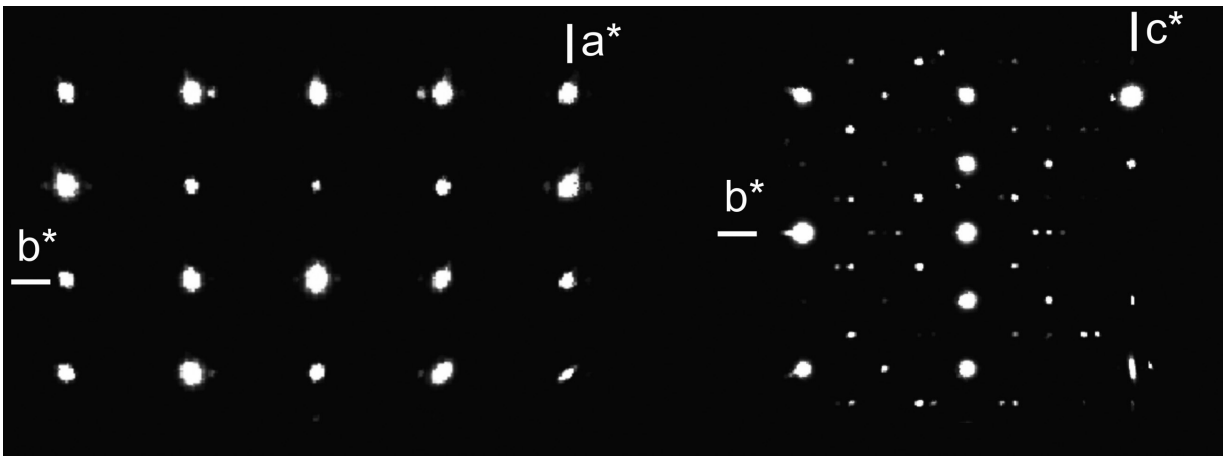

Figure 2. A portion of simulated X-ray precession images for the *hk*0 plane (left) and 0*kl* plane (right) showing the presence of a complex pattern of satellite reflections.

Table 2. Crystal data and structure-refinement information.

	Crystal data
Crystal size (mm)	0.26 × 0.15 ×0.09
a (Å)	7.9979(3)
b (Å)	5.8003(2)
c (Å)	7.2299(2)
β (°)	104.7398(9)
Volume (Å^3)	324.36(2)
Z	1
Space group	$P\,2_1/m$
Wavelength Mo*K*α (Å)	0.7107
Absorption coefficient (mm^{-1})	1.23
Sample-to-detector distance (mm)	50
Scan mode	ω
Scan width (º)	0.3
Acquisition times (s)	20
Collected reflections	8467
Unique reflections	2089
Reflection with ($I \geq 2\ \sigma(I)$)	1984
R_{int}	0.028
θ range (º)	2 – 40
h range	–14 → 13
k range	–10 → 9
l range	–13 → 13
Completeness (%)	96.9
F_{000} (e^-)	342.0
Largest diff. peak / hole (e Å^{-3})	0.49 / -0.70
R_1 / wR_2 ($I \geq 2\ \sigma(I)$)	0.024 / 0.062
R_1 / wR_2 (all data)	0.025 / 0.063
Gof	1.121

collected using a Bruker Hyperion 2000 FTIR microscope equipped with a liquid-nitrogen-cooled MCT detector, KBr beam splitter and a DLATGS detector over the range of 4000-400 cm^{-1} by averaging 100 scans at an operating resolution of 4cm^{-1}. Baseline corrections were done using the OPUS spectroscopic software (Bruker, 2004) and the spectrum was cut to highlight signal in the principal (OH)-stretching region from ~3600-2950 cm^{-1}. The spectrum was fit by Gaussian curves with identical FWHM (full-width-at-half-maximum) values using FITYK V0.9.8 software (Wojdyr, 2010) and the minimum number of curves needed to produce a reasonable fit to the observed data (weighted sum of squared residuals = 0.00234). The fitted spectrum is shown in Figure 4 and details regarding the fitted spectrum are given in Table 6.

RESULTS AND DISCUSSION

Description of the crystal structure

The crystal structure of yoderite consists of chains of edge-sharing A(1)O_5(OH) octahedra parallel to the **b**-direction. The chains are linked by isolated SiO_4 tetrahedra and A(2)O_4(OH) and A(3)O_5 trigonal bipyramids (Figure 3). There are five independent cation sites, eight anion sites, and one hydrogen site. The anion sites are fully occupied by oxygen; the O(5) and O(8) anions are [4]–coordinated whereas the remaining anions are [3]-coordinated. At the O(8) site, the donor oxygen of the OH group bonds to the A(1) and A(2) cations, and the associated H-atom hydrogen-bonds to the O(6) anion (Figure 3). The geometrical features of the O(8)–H···O(6) arrangement are reported in Table 4.

The yoderite structure contains three independent A sites, A(1), A(2) and A(3), occupied principally by Al. The A(1) site is surrounded by five oxygen atoms and one OH group, forming a distorted A(1)O_5(OH) octahedron

Table 3. Atom fractional coordinates, site occupancies and equivalent isotropic-displacement parameters U_{eq} (**Å²**) for yoderite.

Site	Occupancy	*x*/*a*	*y*/*b*	*z*/*c*	U_{eq}
A(1)	$Al_{0.75}Mg_{0.25}$	0.29511(3)	0.00527(4)	0.17753(3)	0.00605(6)
A(2)	$Al_{0.50}Mg_{0.50}$	0.38908(4)	¼	0.62981(5)	0.00638(7)
A(3)	$Al_{0.94(1)}Fe_{0.06(1)}$	0.05545(4)	¼	0.35427(4)	0.00635(9)
Si(1)	$Si_{1.00}$	0.06291(4)	¼	0.79844(4)	0.00648(6)
Si(2)	$Si_{1.00}$	0.33950(4)	¾	0.80271(4)	0.00740(7)
O(1)	$O_{1.00}$	0.05683(7)	0.98004(10)	0.21532(9)	0.00938(10)
O(2)	$O_{1.00}$	0.54626(9)	1.02404(12)	0.21992(10)	0.01514(12)
O(3)	$O_{1.00}$	0.14594(11)	¼	0.61544(11)	0.00978(13)
O(4)	$O_{1.00}$	0.22111(11)	¼	0.99216(11)	0.01026(13)
O(5)	$O_{1.00}$	0.29888(11)	¼	0.36024(12)	0.01121(14)
O(6)	$O_{1.00}$	0.16543(11)	¾	0.63236(12)	0.01044(13)
O(7)	$O_{1.00}$	0.28340(11)	¾	0.00465(12)	0.01270(15)
O(8)	$O_{1.00}$	0.36243(12)	¾	0.36109(12)	0.01331(15)
H	$H_{1.00}$	0.303(3)	¾	0.437(3)	0.0171*

* constrained to be 1.3 times U_{eq} of O(8) atom site.

Table 4. Selected bond distances (Å), angles (°), polyhedron volumes (Å³), polyhedron angle variances (°²), quadratic elongations, mean square deviation from the average bond distances Δ (Å²x10⁴) for yoderite.

A(1)		A(2)		A(3)	
A(1)–O(7)^{3}	1.9245(6)	A(2)–O(5)	1.8983(10)	A(3)–O(6)^{2}	1.7936(9)
A(1)–O(5)	1.9341(6)	A(2)–O(2)^{8,4}	1.9205(8)	A(3)–O(3)	1.8422(9)
A(1)–O(4)^{1}	1.9385(6)	A(2)–O(3)	1.9208(9)	A(3)–O(1)^{3,7}	1.8619(6)
A(1)–O(2)^{3}	1.9563(7)	A(2)–O(8)^{4}	1.9717(10)	A(3)–O(5)	1.9364(9)
A(1)–O(8)^{3}	1.9698(6)	<A(2)–O>	1.9264	<A(2)–O>	1.8592
A(1)–O(1)^{3}	1.9983(6)	Volume	6.008(3)	Volume	5.442(3)
<A(1)–O>	1.9536	Δ × 10^{4}	1.595	Δ × 10^{4}	6.151
Volume	9.672(4)				
OAV	63.127				
OQE	1.019				
Δ×10^{4}	1.622				
Si(1)		Si(2)			
Si(1)–O(3)	1.6244(9)	Si(2)–O(6)	1.6071(9)	O(8)−H	0.81(2)
Si(1)–O(1)^{2,6}	1.6306(6)	Si(2)–O(2)^{5,8}	1.6296(7)	H···O(6)	2.00(2)
Si(1)–O(4)	1.6312(8)	Si(2)–O(7)^{9}	1.6329(9)	O(8)···O(6)	2.8109(12)
<Si(1)–O>	1.6292	<Si(2)–O>	1.6248	O(8)−H···O(6)	177.0000(2)
Volume	2.216(2)	Volume	2.197(2)		
TAV	3.207	TAV	5.096		
TQE	1.001	TQE	1.001		
Δ×10^{4}	0.030	Δ×10^{4}	0.405		

TAV = Tetrahedral Angle Variance; TQE = Tetrahedral Quadratic Elongation; OAV = Octahedral Angle Variance; OQE = Octahedral Quadratic Elongation (Robinson et al., 1971); Δ = mean square relative deviation from the average (Brown and Shannon, 1973).
Symmetry codes: $^{(1)}$*x, y, z*–1; $^{(2)}$–*x*, –*y*+1, –*z*+1; $^{(3)}$*x, y*–1, *z*; $^{(4)}$–*x*+1, –*y*+1, –*z*+1; $^{(5)}$–*x*+1, –*y*+2, –*z*+1; $^{(6)}$–*x, y*–½, –*z*+1, $^{(7)}$*x*, –*y*+¾, *z*; $^{(8)}$–*x*+1, *y*–½, –*z*+1; $^{(9)}$*x, y, z*+1.

Table 5. Anisotropic atom-displacement (Å²) coefficients for yoderite.

Site	U^{11}	U^{22}	U^{33}	U^{23}	U^{13}	U^{12}
A(1)	0.00607(10)	0.00535(10)	0.00650(10)	0.00010(7)	0.00113(7)	0.00033(7)
A(2)	0.00497(13)	0.00739(14)	0.00609(13)	0	0.00019(10)	0
A(3)	0.00641(14)	0.00668(14)	0.00594(13)	0	0.00154(9)	0
Si(1)	0.00581(11)	0.00700(12)	0.00647(11)	0	0.00127(8)	0
Si(2)	0.00679(12)	0.00886(12)	0.00667(11)	0	0.00193(9)	0
O(1)	0.0087(2)	0.0076(2)	0.0117(2)	0.0001(2)	0.0022(2)	-0.0013(2)
O(2)	0.0157(3)	0.0151(3)	0.0176(3)	-0.0066(2)	0.0096(2)	-0.0081(2)
O(3)	0.0102(3)	0.0125(3)	0.0073(3)	0	0.0033(3)	0
O(4)	0.0082(3)	0.0147(3)	0.0070(3)	0	0.0002(3)	0
O(5)	0.0079(3)	0.0132(3)	0.0129(3)	0	0.0036(2)	0
O(6)	0.0085(3)	0.0133(3)	0.0085(3)	0	0.0004(2)	0
O(7)	0.0094(3)	0.0218(4)	0.0071(3)	0	0.0026(2)	0
O(8)	0.0123(3)	0.0197(4)	0.0093(3)	0	0.0053(3)	0

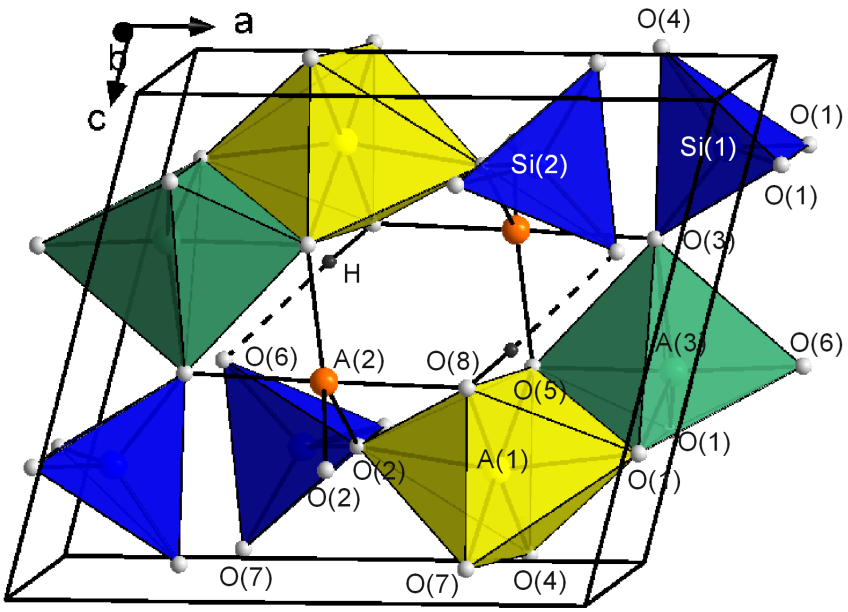

Figure 3. The crystal structure of yoderite projected approximately down [0 1 0], showing the linkage of the chains of $A(1)O_5(OH)$ octahedra with isolated $Si(1)O_4$ and $Si(2)O_4$ tetrahedra and two edge-sharing trigonal bipyramids, $A(2)O_4(OH)$ and $A(3)O_5$.

(OAV 63.13°², OQE 1.019). The <A(1)–O> is 1.954 Å; the grand <$^{[6]}$Al-O> and <$^{[6]}$Mg-O> distances in inorganic structures are 1.903 and 2.089 Å (Gagné and Hawthorne, 2016, 2018), giving a calculated <A(1)–O> distance of 1.950 Å in close accord with the observed value of 1.954 Å. The A(2) and A(3) sites are surrounded by five oxygens in a trigonal bipiramidal arrangement, forming $A(2)O_4(OH)$ and $A(3)O_5$ polyhedra. The Δ values (Table 4) show that the $A(3)O_5$ polyhedron has greater dispersion of the individual bond distances than the $A(2)O_4(OH)$ polyhedron. The observed mean bond distances are 1.926 Å for <A(2)–O> and 1.859 Å for <A(3)–O>, in agreement with their different sites population: ½ Al+½ Mg at A(2) and 0.94 Al+0.06 Fe^{3+} at A(3) atom sites. The

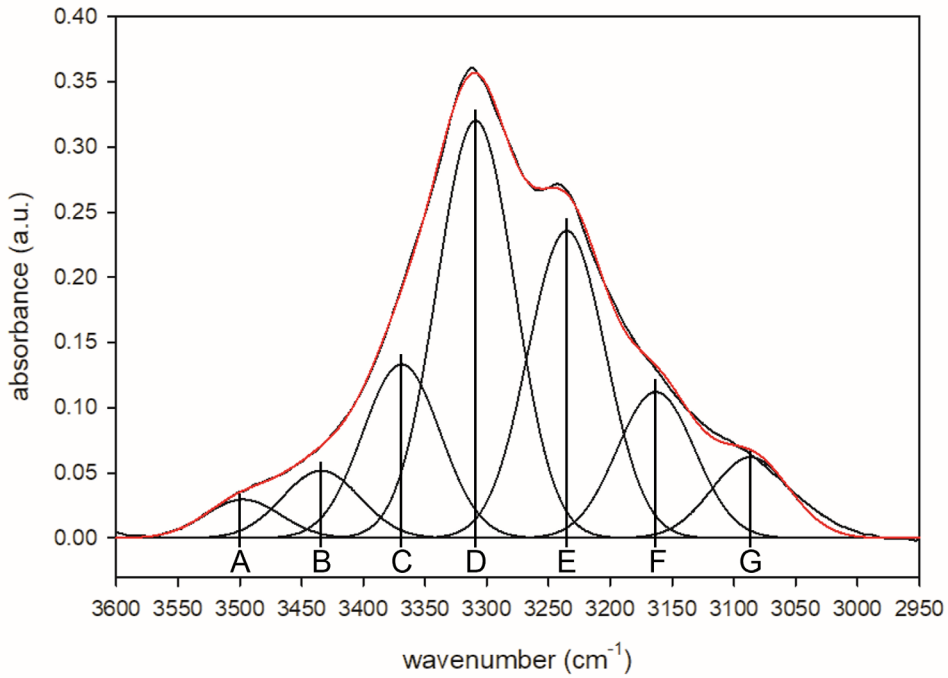

Figure 4. The infrared spectrum in the principal (OH)-stretching region of green yoderite fit with bands A to G. Black curves represent the observed spectra and red curves represent the resultant fit line.

grand <[5]Al-O>, <[5]Mg-O> and <[5]Fe^{3+}-O> distances in inorganic structures are 1.842, 2.044 and 1.966 Å (Gagné and Hawthorne, 2016, 2018, 2020), giving calculated <A(2)–O> and <A(3)–O> distances of 1.943 and 1.849 Å in reasonable accord with the observed values. The two independent Si(1) and Si(2) sites are [4]-coordinated and form two relatively undistorted SiO_4 tetrahedra. The measured <Si–O> values are similar: 1.629 and 1.625 Å, are close to the grand <[4]Si-O> distance of 1.625 Å in inorganic structures (Gagné and Hawthorne, 2018), and correspond to the mean of the two <Si-O> values in andalusite (1.631 Å) and sillimanite (1.627 Å) (Winter and Ghose, 1979).

The calculated bond valence sums (BVS) reported in Table 7 support the proposed site populations for the A and Si sites, and the resulting bond-valence sums are close to the expected values for all sites.

Comparison of purple and green yoderite

The general geometrical features of the structure of green yoderite are consistent with those reported by Fleet and Megaw (1962) and Higgins et al. (1982) for purple yoderite. The green yoderite studied here and the purple sample described in the literature differ only in minor Mn content: green: $(Mg_{2.02}Al_{5.68}Fe^{3+}_{0.35})_{\Sigma 8.05}(Si_{3.93}P^{5+}_{0.03})_{\Sigma 3.96}O_{18}(OH)_2$; purple $(Mg_{1.95}Fe^{2+}_{0.02}Mn^{2+}_{0.01}Fe^{3+}_{0.34}Mn^{3+}_{0.07}Ti_{0.01}Al_{5.57})_{\Sigma 7.97}(Si_{3.98}P^{5+}_{0.03})_{\Sigma 4.01}O_{18.02}(OH)_{1.98}$ (Abu-Eid et al., 1978). Due to the small difference in Mn between green and purple yoderite, there are no discernable differences in the geometrical features of the A polyhedra.

Local clusters in green yoderite and assignment of FTIR bands

Bond-valence analysis (Table 7) shows that O(8) is the donor anion for H which in turn hydrogen-bonds to O(6), and Figure 5 shows the local environment of the H atom. The O(8) anion links to two edge-sharing Al(1) octahedra and one Al(2) trigonal bipyramid, and the hydrogen bond acceptor, O(6), is part of the Si(2) tetrahedron and also bonds to the cations at the A(3) site. Based on the local cluster of NN (nearest-neighbor) polyhedra surrounding O(8) (Figure 5), we may write the following configurational symbol for the environment of the H atom: A(1)A(1)-A(2)-O(8)-H-O(6)-A(3). We may simplify the empirical formula (Table 1) to the following idealized formula: $^{A(1)}(Al_3Mg)_4\ ^{A(2)}(AlMg)_2\ ^{A(3)}(Al^*_2)[Si_4O_{18}(OH)_2]$ where $Al^*=(Al+Fe^{3+})$. Using this formula, we may derive all possible local arrangements as follows:

[1] There is no Mg at A(3), and therefore all arrangements involving the A(3) cation will not affect the number of possible arrangements of cations over the total configuration of sites, ignoring for the moment the presence of Fe^{3+} at the A(3) site.

[2] Al and Mg occupy the A(2) site in a 1:1 ratio, therefore there must be equal numbers of arrangements involving $^{A(2)}$Mg and $^{A(2)}$Al.

[3] Al and Mg occupy the A(1) site in a 3:1 ratio, therefore

Table 6. Band positions, observed intensities and associated local arrangements for green yoderite.

Band	Frequency (cm^{-1})	Obs. Intensity (a.u.)	Arrangement A(1)A(1)-A(2)-A(3)
A	3497.90	3.07	MgMg-Mg-Al
B	3434.13	5.51	MgMg-Al-Al
C	3369.12	14.09	AlMg-Mg-Al
D	3309.04	33.90	AlAl-Mg-Al
E	3235.20	25.00	AlMg-Al-Al
F	3163.12	11.86	AlAl-Al-Al
G	3086.47	6.57	AlAl-Al-Fe^{3+}

$^{A(1)}$(AlAl), $^{A(1)}$(AlMg) and $^{A(1)}$(MgMg) arrangements will occur at the A(1)A(1) edge-sharing dimer in the following proportions for a random distribution (normalized to unity):

$^{A(1)}$(AlAl) = (0.75)(0.75) = 0.5625 = 0.692
$^{A(1)}$(AlMg) = (0.75)(0.25) = 0.1875 = 0.231
$^{A(1)}$(MgMg) = (0.25)(0.25) = 0.0625 = 0.077

[4] Through combination of the dimeric $^{A(1)}$(AlAl), $^{A(1)}$(AlMg) and $^{A(1)}$(MgMg) arrangements with the monomers $^{A(2)}$(Al), $^{A(2)}$(Mg) and $^{A(3)}$Al, the following six complete arrangements are possible:

(1) AlAl-Al-O8-H-O6-Al = AlAl-Al-Al
(2) AlAl-Mg-O8-H-O6-Al = AlAl-Mg-Al
(3) AlMg-Al-O8-H-O6-Al = AlMg-Al-Al
(4) AlMg-Mg-O8-H-O6-Al = AlMg-Mg-Al
(5) MgMg-Al-O8-H-O6-Al = MgMg-Al-Al
(6) MgMg-Mg-O8-H-O6-Al = MgMg-Mg-Al

and to denote these arrangements we will use the short symbols in the form A(1)A(1)-A(2)-A(3) shown to the right above.

If we assume complete short-range disorder of these dimers and monomers, the Al content at the A(1) site (Table 3) suggests that the most intense peak should correspond to arrangement (1) which should occur at the lowest wavenumber. Bands that correspond to arrangements with progressively more Mg should occur at relatively higher wavenumbers and should be less intense due to the lesser abundance of Mg. Examination of Figure 4 shows that this model is obviously not the case, and indicates that $^{A(2)}$Al and $^{A(2)}$Mg must be preferentially associated with certain $^{A(1)}$(AlAl), $^{A(1)}$(AlMg) and $^{A(1)}$(MgMg) dimers.

To get a sense of such ordering trends, we calculated the bond-valence sums at each of the O(1) to O(8) sites for each of the above A(1)A(1)-A(2)-A(3) short-range arrangements (Table 8, upper section); some of these values result in very low bond-valence sums at anions not involved in bonding with the H atom, specifically O(4), O(5) and O(7) (bold italicized values in Table 8), and hence these arrangements are not favoured in terms of the valence-sum rule (Brown, 2016) and hence are less likely to occur. To calculate the bond-valence sums at the O(6) and O(8) atoms, we assumed agreement with the valence-sum rule at O(8) and H, and calculated the resultant O(6)-H bond-valences and bond-valence sums (Table 8, lower section). The bond valences of the optimum arrangements (from a bond-valence perspective) are shown in bold:

Table 7. Bond-valences (in valence units, *vu*) in yoderite.

Atom Site and site charge	Si(1) 4.00	Si(2) 4.00	A(1) 2.74	A(2) 2.50	A(3) 3.00	H(1) 1.00	**Σ** oxygens
O(1)	0.98↓x2		0.41		0.58↓x2		1.97
O(2)		0.99↓x2	0.46	$0.52^{\downarrow x2}$			1.97
O(3)	1.00			0.52	0.61		2.13
O(4)	0.98		$0.48^{\rightarrow x2}$				1.94
O(5)			$0.49^{\rightarrow x2}$	0.56	0.47		2.01
O(6)		1.05			0.69	0.19	1.93
O(7)		0.98	$0.50^{\rightarrow x2}$				1.98
O(8)			$0.44^{\rightarrow x2}$	0.45		0.81	2.14
Σ cations	3.94	4.01	2.78	2.57	2.93	1.00	

Note: The valence of each site takes account of the contribution of different atom species; bond valences were calculated using the bond-valence parameters of Brese and O'Keeffe, 1991.

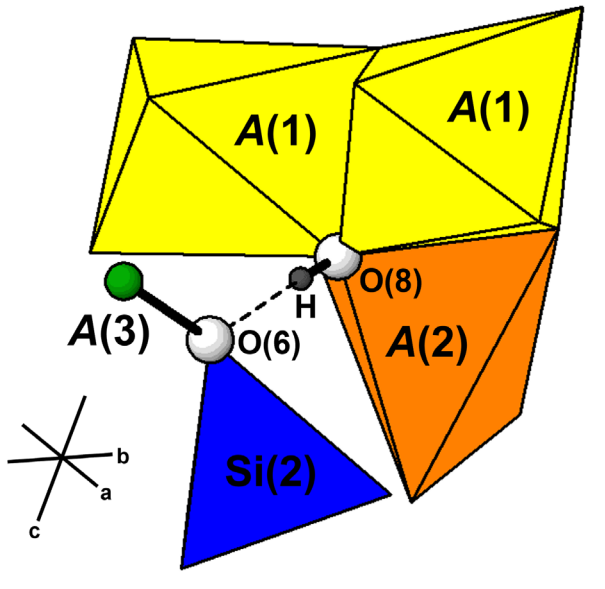

Figure 5. The local environment of the H atom in green yoderite.

AlAl-Mg-Al and AlMg-Al-Al. These two optimum arrangements (AlAl-Mg-Al and AlMg-Al-Al) have strong hydrogen bonds that accord with the low stretching frequences (~3200-3300 cm^{-1}) of the most intense bands in the infrared spectrum (Figure 4). If we consider these two clusters in equal amounts, the aggregate composition is as follows: $[AlAl\text{-}Mg\text{-}Al^*]_{0.5}$ and $[AlMg\text{-}Al\text{-}Al^*]_{0.5}$= $[Al_3Mg][AlMg][Al^*_2]$ which is close to the exact site occupancies (Table 3) and the chemical formula of the crystal (Table 1). This accord suggests that the bond-valence requirements of the short-range arrangements are dictating the chemical composition of the crystal.

Assigning the clusters AlAl-Mg-Al and AlMg-Al-Al to the two most intense bands, D and E (Figure 4), the bands at higher wavenumbers: A, B and C, can be assigned to the less-favored arrangements MgMg-Mg-Al*, MgMg-Al-Al* and AlMg-Mg-Al* as the lighter cations will displace the stretching bands to higher wavenumbers. This leaves the bands F and G to be assigned, and there is one cluster remaining: AlAl-Al-Al*, and the high valence of these cations are in accord with the low wavenumbers of these bands. How can there be two bands assigned to one cluster? We suggest that Fe^{3+} locally orders at A(3) in the AlAl-

Table 8. Short-range bond-valence sums (vu) at the anions in green yoderite.

	Incident bond-valence sums (vu) from the various local A(1)A(1)-A(2)-A(3) arrangements*					
	AlAl-Al-Al	AlAl-Mg-Al	MgMg-Al-Al	AlMg-Mg-Al	AlMg-Al-Al	MgMg-Mg-Al
O(1)	2.09	2.09	1.92	2.01	2.01	1.92
O(2)	2.09	1.89	1.92	1.81	2.01	1.65
O(3)	2.20	2.00	2.20	2.00	2.20	1.80
O(4)	1.98	1.98	***1.64***	***1.64***	1.82	***1.64***
O(5)	2.20	2.00	1.86	***1.56***	2.04	***1.56***
O(6)	1.65	1.65	1.65	1.65	1.65	1.65
O(7)	1.98	1.98	***1.64***	1.96	1.82	***1.64***
O(8)	*1.60*	1.40	1.26	1.24	1.44	1.06
	Incident bond-valence (vu) sums** at the O(6) and O(8) anions from both local A(1)A(1)-A(2)-A(3) arrangements and the O_{donor}-H and H…$O_{acceptor}$ bonds***					
O(6)	1.65+0.60	**1.65+0.40**	1.65+0.26	1.65+0.24	**1.65+0.44**	1.65+0.06
O(8)	1.60+0.40	**1.40+0.60**	1.26+0.74	1.24+0.76	**1.44+0.56**	1.06+0.94
	Incident bond-valence (vu) sums** at the O(6) anion for all combinations of local A(1)A(1)-A(2)-A(3) arrangements and ideal O(8) bond-valence (vu) sums.					
O(6)	***2.25***	**2.05**	1.91	1.89	**2.09**	***1.71***

*columns containing low (bold italicized) bond-valence sums cannot be stable arrangements;

**columns containing close-to-ideal (bold) bond-valence sums can be stable arrangements;

***O_{donor}-H bond-valences were calculated for ideal bond-valence sums at the O(8) and H atoms.

Al-Al* cluster, giving the local arrangements AlAl-Al-Al and AlAl-Al-Fe^{3+} and the bands F and G, respectively. The band positions, observed intensities and the assigned local atomic arrangements are given in Table 6.

Variation in band intensities

The relation of observed band intensities in the principal-stretching regions of the infrared to the frequency of occurrence of the associated local atomic arrangements is not straightforward. Skogby and Rossman (1991) state that "Polarized IR spectra of single-crystals of amphiboles show that the molar absorptivity of the fundamental vibrational OH band is strongly wavenumber dependent". The analogous relation was observed in polarized single-crystal spectra of vesuvianite (Groat et al., 1995). On the other hand, Della Ventura et al. (1993) showed that in the powder infrared spectra of synthetic (Ni,Mg,Co)-potassium-richterite solid-solutions, the relative intensities of the four bands due to the *M*(1)*M*(1)*M*(3) arrangements MgMgMg, MgMgNi, MgNiNi and NiNiNi (and their Co analogues) are independent of band frequency (wavenumber) and are dependent solely on the site populations of the *M*(1) and *M*(3) sites which had been determined previously by Rietveld refinement (Della Ventura et al., 1993).

Do the findings of Skogby and Rossman (1991) and Della Ventura et al. (1996) contradict each other? Skogby and Rossman (1991) determined the aggregate intensity of all *M*(1)*M*(1)*M*(3) bands for a series of amphiboles of different composition, whereas Della Ventura et al. (1993) determined the individual intensities of all four *M*(1)*M*(1)*M*(3) bands in each single amphibole of the solid-solution series. Thus the answer to the above question is "no", the results do not contradict each other. In each amphibole, the relative molar absorptivities of the four *M*(1)*M*(1)*M*(3) bands are the same, but in each different amphibole, the molar absorptivity is different as the mean band frequency is different. Burns and Hawthorne (1994) showed that the normalized OH-stretching-band intensities in the powder infrared spectrum of the ordered borate mineral preobrazhenskite are a linear function of band frequency. The key issue in preobrazhenskite is that the OH groups in the structure are spatially separated. In amphiboles, the *M*(1)*M*(1) part of a cluster has two (OH) groups at the end of the shared edge, and these (OH) groups belong to different clusters with different *M*(3) cations but the same *M*(1)*M*(1) cations (Figure 6a). Thus it is not surprising to find that the vibrations of the (OH) groups are strongly correlated in single infrared spectra, to the extent that they have the same molar absorptivity despite differences in local cation composition.

Now let us consider the A(1)A(1)-A(2) cluster in yoderite (Figure 6b). Although adjacent clusters link through a shared edge, they do not have any constituent cations in common, and hence seem unlikely to couple. Thus, the molar absorptivities of each band will be different as the absorption energies are different. As a result of this difference in molar absorptivities, we do not expect a 1:1 relation between band intensity and the frequency of occurrence of the local cluster giving rise to each band. Thus, although we know the approximate abundances of each of the clusters in the assigned spectrum (Figure 4), we cannot assign accurate abundances without knowing the variation in molar absorptivity as a function of band frequency (wavenumber).

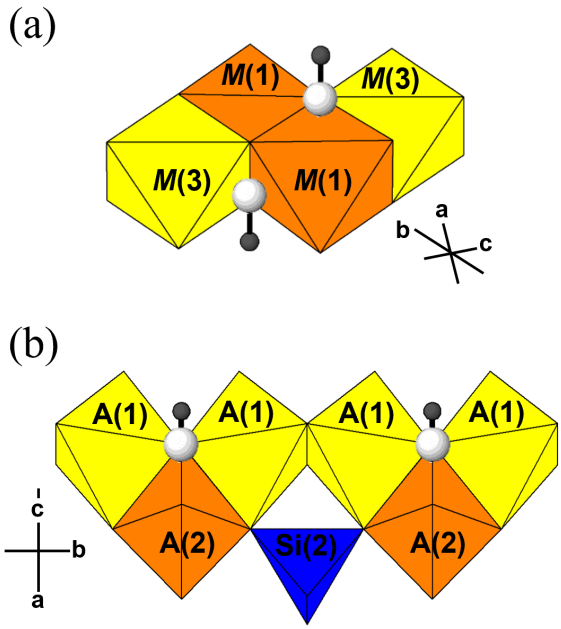

Figure 6. Adjoining local clusters of polyhedra associated with the H atom in (a) tremolite (Hawthorne and Grundy, 1976), and (b) green yoderite.

ACKNOWLEDGEMENTS

The authors are indebted with Gunnar Färber who provided the sample with green crystals of yoderite. This work was supported by the Ministero dell'Istruzione, dell'Università e della Ricerca and by the University of Pavia, and by a Discovery Grant to FCH from the Natural Sciences and Engineering Council of Canada and a Canada Foundation of Innovation Grant to FCH.

REFERENCES

Abu-Eid R.M., Langer K., Seifert F., 1978. Optical Absorption and Mossbauer Spectra of Purple and Green Yoderite, a Kyanite-Related Mineral. Physics and Chemistry of Minerals 3, 271-289.

Brese N.E. and O'Keeffe M., 1991. Bond-valence parameters for solids. Acta Crystallographica B47, 192-97.

Brown I.D. and Shannon R.D., 1973. Empirical bond-strength-bond-length curves for oxides. Acta Crystallographica A29, 266-282.

Brown I.D., 2016. The Chemical Bond in Inorganic Chemistry: The Bond Valence Model, 2nd edition. Oxford University Press.

Bruker, 2003. SAINT Software reference manual, version 6. Bruker AXS Inc., Madison, Wisconsin, (USA).

Bruker, 2004. OPUS Spectroscopic Software Reference Manual, OPTIK GmbH, Rudolf-Plank-Straße 27, D-76275, Ettlingen.

Burns P.C. and Hawthorne F.C., 1994. Structure and hydrogen bonding in preobrazhenskite, a complex heteropolyhedral borate. Canadian Mineralogist 32, 387-396.

Della Ventura G., Robert J.-L., Raudsepp M., Hawthorne F.C., 1993. Site occupancies in monoclinic amphiboles: Rietveld structure refinement of synthetic nickel magnesium cobalt potassium richterite. American Mineralogist 78, 633-640.

Fleet S.G. and Megaw H.D., 1962. The Crystal Structure of Yoderite. Acta Crystallographica 15, 721

Fockenberg T. and Schreyer W., 1991. Yoderite, a mineral with essential ferric iron: Its lack of occurrence in the system MgO–Al_2O_3–SiO_2–H_2O. American Mineralogist 76, 1052-1060.

Gagné O. and Hawthorne F.C., 2016. Bond-length distributions for ions bonded to oxygen: alkali and alkaline-earth metals. Acta Crystallographica B72, 602-625.

Gagné O.C. and Hawthorne F.C., 2018. Bond-length distributions for ions bonded to oxygen: Metalloids and post-transition metals. Acta Crystallographica B74, 63-78.

Gagné O.C. and Hawthorne F.C., 2020. Bond-length distributions for ions bonded to oxygen: Results for the transition metals and quantification of the factors underlying bond-length variation in inorganic solids. IUCrJ 7, 581-629.

Gaines R.V., Skinner H.C.W., Foord E.E., Mason B., Rosenzweig A., 1997. Dana's New Mineralogy. Eighth Edition. New York and Chichester (JohnWiley and Sons, Ltd.). IBSN 0–471–19310–0.

Groat L.A., Hawthorne F.C., Rossman G.R., Ercit T.S., 1995. The infrared spectroscopy of vesuvianite in the OH region. Canadian Mineralogist 33, 609-626.

Hawthorne F.C. and Grundy H.D., 1976. The crystal chemistry of the amphiboles. IV. Xray and neutron refinements of the crystal structure of tremolite. Canadian Mineralogist 14, 334-345.

Higgins J.B., Ribbe P.H., Nakajima Y., 1982. An ordering model for the commensurate antiphase structure of yoderite. American Mineralogist 67, 76-84.

Higgins J.B. and Ribbe P.H., 1977. The crystal structure and domain texture of yoderite. Geological Society of America Abstracts with Programs 9, 1015.

Ibers J.A. and Hamilton W.C., 1992. International Tables for X-ray Crystallography, Vol. C. Dordrecht: D. Reidel Publishing.

Johnson S.P. and Oliver G.J.H., 1998. A second natural occurrence of yoderite. Journal of Metamorphic Geology 16, 809-818.

Krause L., Herbst-Irmer R., Sheldrick G.M., Stalke D., 2015. Comparison of silver and molybdenum microfocus X-ray sources for single-crystal structure determination. Journal of Applied Crystallography 48, 3-10.

Lefebvre A., 1982. Lattice defects in three structurally related mineral: kyanite, yoderite and staurolite. Physics and Chemistry of Minerals 8, 251-256

Li D., Peng M., Murata T., 1999. Coordination and local structure of magnesium in silicate minerals and glasses: Mg K-edge Xanes study. The Canadian Mineralogist 37, 199-206.

McKie D. and Bradshaw N., 1966. Green variety of yoderite. Nature 210, 1148.

McKie D., 1959. Yoderite, a new hydrous magnesium iron aluminosilicate from Mautia Hill, Tanganyika. Mineralogical Magazine 32, 282-307.

Mruma A.H. and Basu N.K., 1987. Petrology of the talc-kyanite-yoderite-quartz schist and associated rocks of Mautia Hill, Mpwapwa District, Tanzania. Journal of African Earth Sciences 6, 301-311.

Pouchou J.L. and Pichoir F., 1985. 'PAP' (φρZ) procedure for improved quantitative 513 microanalysis, 104-106. In: Microbeam Analysis (J.T. Armstrong, editor). San 22 514 Francisco Press, San Francisco, California, USA.

Ribbe P.H., Nakajima Y., Higgins J.B., 1981. Modulated structures in mullite and yoderite. Geological Society of America Abstracts with Programs, l3, 537.

Robinson K., Gibbs G.V., Ribbe P.H., 1971. Quadratic elongation, a quantitative measure of distortion in coordination polyhedra. Science 172, 567-570.

Schreyer W. and Seifert F., 1969. Compatibility relations of the aluminum silicates in the systems MgO–Al_2O_3–SiO_2–H_2O and K_2O–MgO–Al_2O_3–SiO_2–H_2O at high pressures. American Journal of Science 267, 371-88.

Sheldrick G.M., 2015. Crystal structure refinement with SHELXL. Acta Crystallographica C71, 3-8.

Skogby H. and Rossman G.R., 1991. The Intensity of amphibole OH bands in the infrared absorption spectrum. Physics and Chemistry of Minerals 18, 64-68.

Winter K.J. and Ghose S., 1979. Thermal expansion and high-temperature crystal chemistry of the Al_2SiO_5 polymorphs. American Mineralogist 64, 573-586.

Wojdyr M., 2010. Fityk: a general-purpose peak fitting program. Journal of Applied Crystallography 43, 1126-11284.

CC BY This work is licensed under a Creative Commons Attribution 4.0 International License CC BY. To view a copy of this license, visit http://creativecommons.org/licenses/by/4.0/